Title

Introducing Solubility Control for Improved Organic P-Type Dopants

Journal

Chemistry of Materials, 27(16)

ISSN

0897-4756

Authors

Li, Jun

Zhang, Guangwu

Holm, Daniella M

et al.

Publication Date

2015-08-25

DOI

10.1021/acs.chemmater.5b02340

Peer reviewed

CHEMISTRY OF MATERIALS

Article

pubs.acs.org/cm

Introducing Solubility Control for Improved Organic P-Type Dopants

Jun Li,[†,‡] Guangwu Zhang,[†,§] Daniella E. Holm,[‡] Ian E. Jacobs,[‡] Bin Yin,[§] Pieter Stroeve,[‡] Mark Mascal,*[,§] and Adam J. Moulé*[,‡]

[‡]Department of Chemical Engineering and Materials Science and [§]Department of Chemistry, University of California, Davis, United States

Supporting Information

ABSTRACT: To overcome the poor solubility of the widely used p-type dopant 2,3,5,6-tetrafluoro-7,7,8,8-tetracyanoquinodimethane (F4TCNQ), we have synthesized a series of structure-modified, organic p-type dopants to include alkyl ester groups designed to enable solubility and miscibility control. UV−vis−NIR and cyclic voltammetry measurements show increased solubility of mono- and diester substituted dopants with only modest changes to acceptor strength. Using UV−vis−NIR, photoluminescence, and in-plane conductivity measurements, we demonstrate that the new dopants can successfully p-type dope poly(3-hexylthiophene-2,5-diyl) (P3HT). Monoester substituted dopants are characterized by only slightly reduced electron affinity relative to F4TCNQ, but greater doping effectiveness due to increased miscibility with P3HT. Diester substituted dopants undergo a dimerization reaction before assuming their doped states, which may help anchor dopants into position post deposition, thus decreasing the negative effect of dopant drift and diffusion. We conclude that increased dopant solubility/miscibility increases the overall effectiveness of doping in solution-cast polymer films and that ester modification is a practical approach to achieving solubility/miscibility control in TCNQ-type dopants.

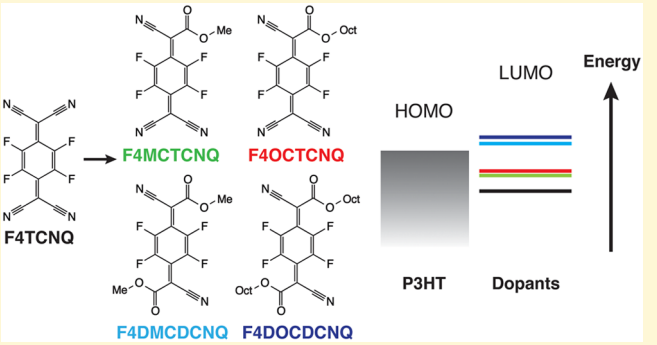

INTRODUCTION

Organic semiconductors have recently drawn much interest because of a number of advantages they have over conventional inorganic materials, which may include low cost, light weight, compatibility with flexible substrates, biocompatibility, low environmental impact, and chemical tailorability.[1−4] Organic electronic devices, such as organic light-emitting diodes (OLEDs),[5,6] organic photovoltaics (OPV)[7,8] and organic field-effect transistors (OFETs),[9,10] show significant improvements in performance with the addition of dopants. Intrinsic organic semiconductors in general have low free-charge densities and therefore low conductivity compared to inorganic semiconductors. To increase conductivity, conjugated polymers or small molecule semiconductors can be doped via the addition (n-type) or removal (p-type) of electrons. One method of doping a polymer is to form an organic salt using acidic or basic doping groups for p- and n-type doping, respectively.[11] Polyethylenedioxythiophene polystyrenesulfonate (PEDOT:PSS) is a well-known example of an acidically doped p-type organic conductive material.[12,13] An alternative method to dope organic semiconductors is to add a neutral molecule with an electron affinity (EA) higher than the ionization energy (IE) of the organic semiconductor.[14] In this case, an electron from the semiconductor is spontaneously donated to the high EA molecule to create a hole state, a classic example being the use of iodine to dope polythiophenes.[15,16]

High EA organic molecular dopants have been studied since the 1960s. Recent studies on such dopants have focused on the role that ground state and excited state charge transfer (CT) states play in quenching excited state fluorescence and in recombination processes in OPV devices.[17−20] Assuming no CT-state formation, charge transfer occurs when the lowest unoccupied molecular orbital (LUMO) of the dopant is accessible to the highest occupied molecular orbital (HOMO) of the organic semiconductor matrix. The dopant molecule must also have a stable structure that can be reoxidized without reaction with nearby molecules. The quinone structure has these characteristics and early studies of molecular organic dopants focused on tetrachlorobenzoquinone (chloranil; LUMO: −2.76 eV)[21−23] and tetracyanoquinodimethane (TCNQ; LUMO: −2.8 eV).[24,25] More recently, dopants with higher EA were prepared by incorporating electron-withdrawing groups into the quinone ring. Dopants in this category include 2,3-dichloro-5,6-dicyano-1,4-benzoquinone (DDQ; LUMO: −4.6 eV)[26−28] and the more widely used 2,3,5,6-tetrafluoro-7,7,8,8-tetracyanoquinodimethane (F4TCNQ; LUMO: −5.24 eV).[14,29,30] Following the same concept of molecular design, even higher EA dopants, such as 1,3,4,5,7,8-hexafluorotetracyanonaphthoquinodimethane (F6-

Received: June 18, 2015
Revised: July 20, 2015

DOI: 10.1021/acs.chemmater.5b02340
Chem. Mater. XXXX, XXX, XXX−XXX

TNAP; LUMO: −5.37 eV)[31,32] and 3,6-difluoro-2,5,7,7,8,8-hexacyanoquinodimethane (F2-HCNQ; LUMO: −5.59 eV),[33] have been recently synthesized. Other recently reported p-type dopants with high EA include C_{60} fullerene (LUMO: −3.6 eV),[34] its fluorinated derivative $C_{60}F_{36}$ (LUMO: −5.38 eV),[35,36] and hexaazatriphenylene hexacarbonitrile (HAT-CN6; LUMO: 5.7 eV).[37−39] However, most of these dopants have low solubility in common solvents, and are incorporated into devices structures using either evaporation processes[14,40] or premixing in an inert matrix[41] because they cannot be effectively solution processed. This limitation significantly restricts further development of solution-processed and mass-produced organoelectronics applications.[42]

In this paper, we first demonstrate a straightforward synthetic route to soluble versions of F4TCNQ-type dopants by substituting the cyano groups with either methyl or n-octyl esters (Figure 1). A comprehensive study of the electro-

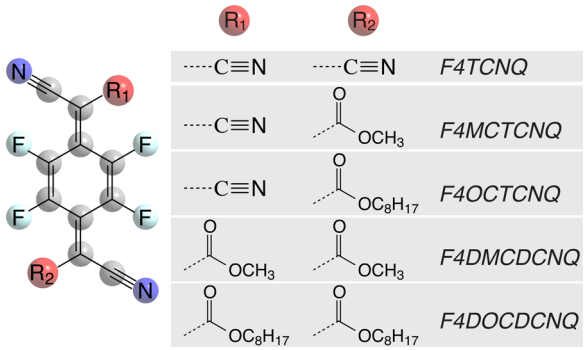

Figure 1. Molecular structures of F4TCNQ and its ester analogues.

chemical properties of these F4TCNQ analogues is performed using cyclic voltammetry. With a combination of optical absorption spectroscopy, photoluminescence spectroscopy, and conductivity measurements, we not only demonstrate the p-type doping of P3HT using these new dopants, but also show that comparable doping efficiency can be achieved even with slightly reduced electron affinity. These novel molecular dopants establish that the introduction of solubility control is a successful strategy to tailor the properties of organic p-type dopants.

EXPERIMENTAL SECTION

Materials. 1,4-Bis(chloromethyl)-2,3,5,6-tetrafluorobenzene was purchased from Oakwood Products. Sodium hydride (60% dispersion in mineral oil) was purchased from Alfa Aesar. Bromine, perfluorobenzene, potassium carbonate, dimethyl carbonate, malononitrile, sodium acetate, sodium hydroxide, and phosphorus tribromide were purchased from Sigma-Aldrich. Anhydrous dimethyl sulfoxide (DMSO) and dimethylformamide (DMF) were purchased from Acros Organics. Hydrochloric acid (37% aqueous), p-toluenesulfonic acid monohydrate, ethanol, tetrahydrofuran (THF), dichloromethane (DCM), ethyl acetate, toluene, and hexane were purchased from Fisher Scientific. Acetic acid and sodium cyanide were purchased from Fluka. Octanol was purchased from EM Science. Trifluoroacetic acid (TFA) and acetic anhydride were purchased from EMD. P3HT (Regioregular >98%, M_n = 54−75 kDa, HOMO 5 eV and LUMO 3 eV) was purchased from Sigma-Aldrich. F4TCNQ (>98%) was purchased from TCI. All chemicals were used as received unless otherwise indicated. All solvents were dried over molecular sieves (3 Å) before use.

Characterization. ^{1}H NMR (300 MHz), ^{13}C NMR (75 MHz) and ^{19}F-NMR (282 MHz) spectra were recorded on a Varian Mercury 300 NMR spectrometer. Spectral data were processed using MestReNova (version 6.2.0) desktop NMR data processing software.

Cyclic voltammograms (CVs) were recorded on a BASi Epsilon MF-9092 Electrochemical Workstation. The redox potentials of all of substrates were measured in anhydrous acetonitrile (MeCN) solution containing tetramethylammonium tetrafluoroborate (Me_4NBF_4, 0.05M) using a platinum disk (Φ = 1.6 mm) as the working electrode and Ag/AgCl as the reference electrode. The concentration of substrates in the working solution was 0.5 mM, and the electrochemical potential sweep rate was fixed at 100 mV/s.

High resolution mass spectra (HRMS) were obtained on a Thermo Fisher Hybrid LTQ-Orbitrap XL mass spectrometer equipped with electrospray. Liquid chromatography−mass spectra (LC-MS) were recorded on Qtrap LC/MS instruments.

UV−vis−NIR and photoluminescence spectra were recorded on a PerkinElmer Lambda 750 spectrophotometer and a Varian Eclipse photoluminescence spectrophotometer, respectively. For the solubility measurements, 5 mg of F4TCNQ and 100 mg of the four new dopants were introduced into 1.0 mL of chloroform. The mixtures were stirred on a hot plate at 60 °C for 24 h, and then rested at room temperature for another 24 h. Saturated solutions were diluted accordingly in order to be measured in a useful absorbance range. Calibration curves were also measured for each dopant. For characterization of the blended films, glass substrates were cleaned in ultrasonic baths of acetone, Mucasol detergent (5%), and deionized water, followed by drying with nitrogen. The substrates were then exposed to UV/ozone for 30 min before use. Solutions of 5 mg/mL P3HT and p-type dopants (0.5 mg/mL for F4TCNQ and 5 mg/mL for the ester derivatives) in chloroform were mixed in appropriate ratios to achieve the desired mole fraction of dopants to P3HT. Except neat F4TCNQ, all other films were spin-coated from blend solutions at 60 °C inside a nitrogen glovebox. Neat F4TCNQ films were deposited using an MBruan thermal evaporator at deposit rate ∼0.2 Å/s. Film thicknesses were measured with a Veeco Dektak 150 Surface profilometer. All UV−vis−NIR and photoluminescence spectra were measured under ambient conditions in air.

Conductivity measurements were performed with a four-point probe setup using a Keithely 2420 source sourcemeter unit. Four electrodes (5 nm Cr/95 nm Au, 1 × 5 mm^2, 1 mm spacing) were deposited through a shadow mask by thermal evaporation. The same procedure was used for substrate cleaning and blended film deposition described above. All conductivity measurements were performed in the dark under a nitrogen atmosphere in a glovebox.

RESULTS AND DISCUSSION

Synthesis of P-Type Dopants. Synthesis of the symmetrical di(alkoxycarbonyl)dicyanotetrafluoroquinodimethanes **F4DMCDCNQ** and **F4DOCDCNQ** starts from commercial 1,4-bis(chloromethyl)-2,3,5,6-tetrafluorobenzene **1** (Scheme 1). Conversion to the required bis(cyanomethyl) derivative **3** does not take place by direct substitution with cyanide, so the intermediate bis(bromomethyl)tetra-fluorobenzene **2** was prepared. Remarkably, direct substitution of **1** with bromide also proves challenging, but **2** could be made via the corresponding (bis)benzyl alcohol. Substitution of **2** with cyanide is facile, and methoxycarbonylation of **3** by deprotonation and reaction with dimethyl carbonate gives diester **4**. Oxidation of **4** to the dimethyl ester F4TCNQ analogue **F4DMCDCNQ** with bromine proceeds in high yield. Alternatively, transesterification of **4** with octanol gave the longer-chain diester **5**, which could likewise be readily oxidized to **F4DOCDCNQ**.

The synthesis of the mono(alkoxycarbonyl)-tetrafluorotricyanoquinodimethanes **F4MCTCNQ** and **F4OCTCNQ** starts from commercial hexafluorobenzene (Scheme 2). Reaction with methyl cyanoacetate in the presence of a base gives the intermediate methyl 2-cyano-2-

DOI: 10.1021/acs.chemmater.5b02340
Chem. Mater. XXXX, XXX, XXX−XXX

Scheme 1. Synthesis of F4DMCDCNQ and F4DOCDCNQ[a]

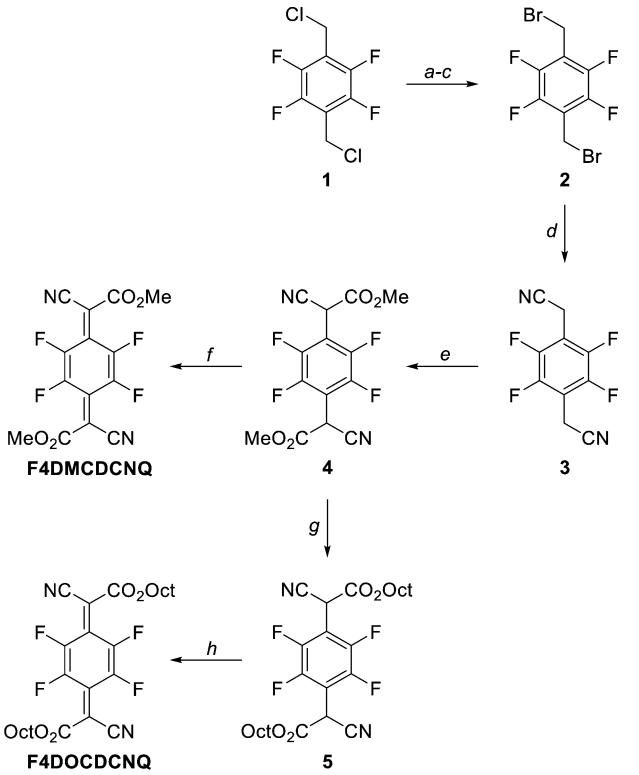

[a]Reagents and conditions: (a) NaOAc, Ac_2O, AcOH, 105 °C, 36 h; (b) NaOH, EtOH/THF/H_2O, 75 °C, 24 h; (c) PBr_3, DCM, 10 h, 76% over 3 steps; (d) NaCN, CF_3COOH, DMSO, 5 h, 51%; (e) $(MeO)_2CO$, NaH, THF, 75 °C, 18 h, 83%;(f) Br_2, H_2O, 2 h, 94%; (g) octanol, TsOH·H_2O, toluene, 110 °C, 6 h, 72%; (h) Br_2, H_2O, 3 h, 93%.

Scheme 2. Synthesis of F4MCTCNQ and F4OCTCNQ[a]

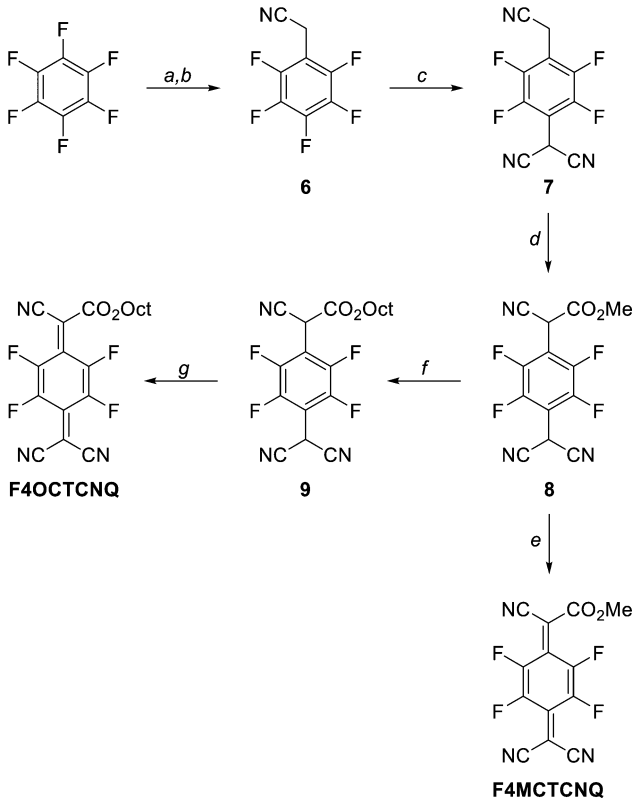

[a]Reagents and conditions: (a) $MeOCOCH_2CN$, K_2CO_3, DMF, 115 °C, 6 h, 72%; (b) 50% aq HOAc, conc. H_2SO_4, reflux, 15 h, 75%; (c) $CH_2(CN)_2$, NaH, THF, 70 °C, 18 h, 66%; (d) $(MeO)_2CO$, NaH, THF, 80 °C, 48 h, 89%; (e) Br_2, H_2O, 1 h, 82%; (f) octanol, TsOH·H_2O, toluene, 85 °C, 9 h, 71%; (g) Br_2, H_2O, 1.5 h, 81%.

(pentafluorophenyl)acetate, which is decarboxylated in situ to give 2-(pentafluorophenyl)ethanenitrile **6**. S_NAr substitution with the sodium salt of malononitrile provides **7**, which is methoxycarbonylated by reaction with dimethyl carbonate and base to give **8**. Oxidation of **8** with bromine gives **F4MCTCNQ**, the monomethyl ester analogue of F4TCNQ. Transesterification of **8** with octanol followed again by oxidation gives the mono-octyl ester dopant **F4OCTCNQ**. Detailed synthetic procedures are provided in the Supporting Information.

Characterization of P-Type Dopants. Our dopant design goal was to improve the solubility of the dopant molecules without compromising doping efficiency. To demonstrate the improved solubility of the new F4TCNQ analogues, saturated solutions were prepared in chloroform (Figure 2a) and their absorbance spectra were recorded by UV−vis−NIR at room temperature. The solubility limits (Figure 2b) were then determined based on calibration curves of each compound. The details of the calibration curves and measurements can be found in the Figure S47. As can be seen from Figure 2b, the solubility of the ester-substituted dopants is significantly greater than F4TCNQ itself, by a factor of at least 55 for F4MCTCNQ and 100 for F4OCTCNQ. Interestingly, although the solubility of the diesters are still ∼30 times higher than that of F4TCNQ, they are less soluble than the monoesters, which is attributed to the higher symmetry of the diesters.[43]

Because the EA of the dopant is an important predictor of doping efficiency, the next thing we needed to show is what effect substitution of an ester group for a cyano group on the F4TCNQ structure would have on the reduction potential. The electrochemical states of the dopants were investigated using cyclic voltammetry (CV). Solutions of dopants in acetonitrile were measured under reducing potentials and the CV data are shown in Figure 3a. As expected, F4TCNQ itself undergoes two reversible one-electron reduction steps corresponding to $F4TCNQ^{\bullet-}$ and $F4TCNQ^{2-}$. The monoester-substituted dopants F4MCTCNQ and F4OCTCNQ also exhibit two reduction peaks, but interestingly, they are located between the first and second reductions of F4TCNQ, and the first reduction peak E_{red1} of the monoester-substituted dopants is greater than the second reduction peak E_{red2}. Unlike F4TCNQ, only one reduction peak is seen in the CV of diester-substituted dopants. Closer inspection of the CV data reveals that both the mono and diesters undergo redox processes that are either irreversible or quasi-reversible. Therefore, instead of using the mean values of anodic and corresponding cathodic peak potentials ($E_{1/2}$), reduction potentials were used for comparison. The reduction potentials for all dopants vs Ag/AgCl are summarized in Table 1.

As can be seen from Table 1, E_{red1} shows a decreasing trend from 0.51 to ∼0.4 and ∼0.2 V as cyano groups are substituted by one or two ester groups, respectively, showing that F4TCNQ is a stronger p-type dopant than its ester analogues. This is expected since the cyano group is more electron withdrawing than the ester group, which results in a more electron deficient quinoid ring in the F4TCNQ than in the

DOI: 10.1021/acs.chemmater.5b02340
Chem. Mater. XXXX, XXX, XXX−XXX

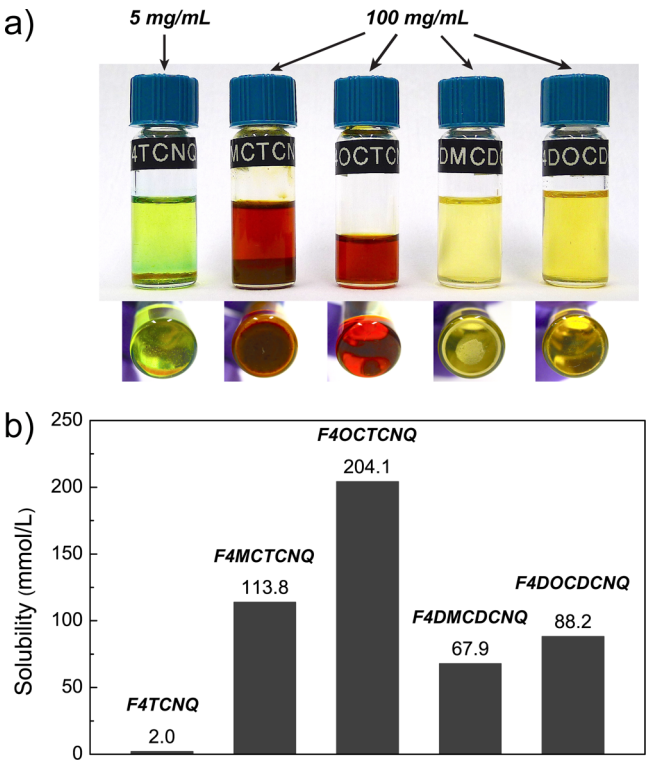

Figure 2. (a) Photos of saturated solutions (from left to right: F4TCNQ, F4MCTCNQ, F4OCTCNQ, F4DMCDCNQ, and F4DOCDCNQ) in chloroform. (b) Measured solubility limits of the dopants in chloroform at room temperature.

Table 1. Summary of Reduction Potentials from CV and Determined LUMO Levels of F4TCNQ and Its Ester Derivatives

compd	E_{red1}(V)	E_{LUMO1}(eV)	E_{red2}(V)	E_{LUMO2} (eV)
F4TCNQ	0.51	−5.23	0	−4.72
F4MCTCNQ	0.42	−5.14	0.12	−4.84
F4OCTCNQ	0.40	−5.12	0.11	−4.83
F4DMCDCNQ	0.25	−4.97		
F4DOCDCNQ	0.21	−4.93		

ester-substituted derivatives. Comparing the octyl and methyl ester substituted dopants, subtle differences in E_{red1} are observed. Longer alkyl chains are more electron donating so the E_{red1} values of the methyl ester-substituted dopants are slightly greater than those of the octyl ester derivatives, increasing from 0.40 to 0.42 V and from 0.21 to 0.25 V, for the monoester and diester derivatives, respectively.

On the basis of the CV data, the LUMO levels for each dopant can be determined from their reduction potentials according to following relationship: $E_{LUMO} = -e(E_{red} + E_{ref})$, where E_{ref} is 4.72 V for the Ag/AgCl reference electrode used in our measurements.[33,44,45] The measured LUMO energies are also listed in Table 1. The measured LUMO level of F4TCNQ (−5.23 eV) is in good agreement with the published values from CV (5.33 eV)[33] as well as ultraviolet photoelectron spectroscopy (UPS) (5.24 eV),[46] which verifies the accuracy of our assignments.

To enable a visual comparison, the LUMO levels of all investigated p-type dopant molecules are compiled into one energy diagram (Figure 3b). The HOMO and LUMO levels of P3HT and P3HT positive polaron ($P3HT^+$) reported from literature[15,47−49] are also shown to scale. Further discussion of

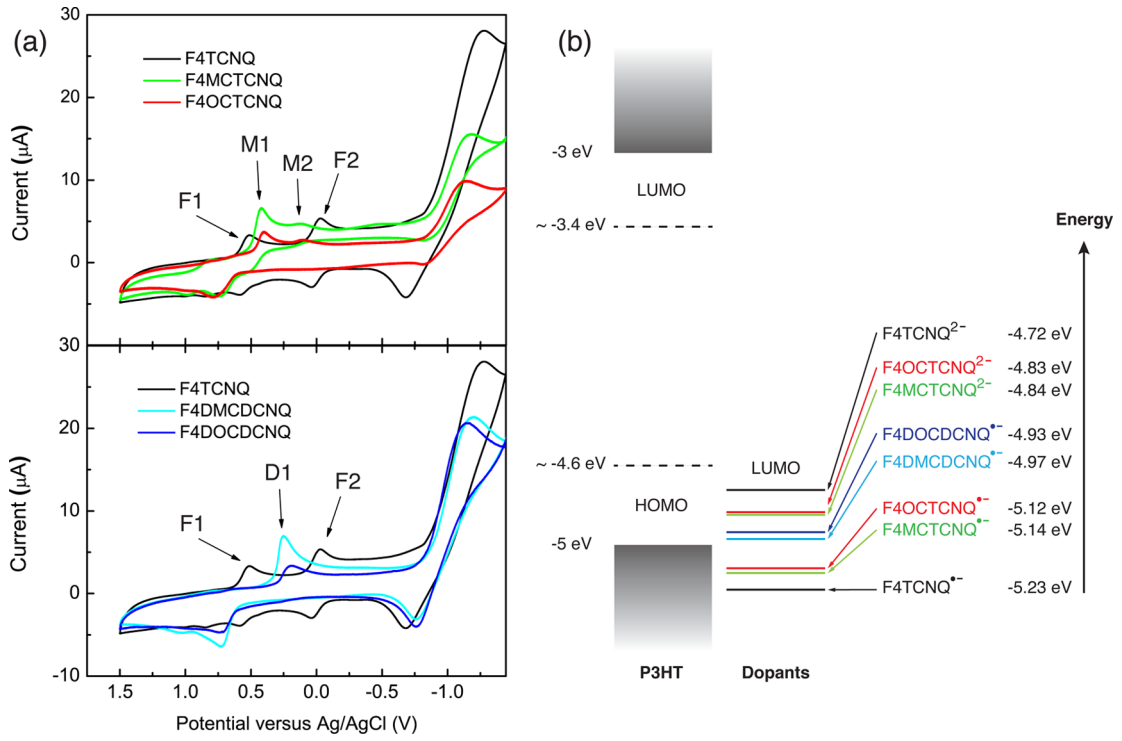

Figure 3. (a) Cyclic voltammograms of F4TCNQ and its monoester derivatives (top) and diester derivatives (bottom). Reduction potentials of F4TCNQ (F1, F2), monoester derivatives (M1, M2), and diester derivatives (D1) are marked. (b) Molecular orbital energy level diagram of P3HT (left: solid line for neutral P3HT and dashed line for P3HT polaron) and p-type dopants (right).

DOI: 10.1021/acs.chemmater.5b02340
Chem. Mater. XXXX, XXX, XXX−XXX

the P3HT matrix/dopants system is deferred to the next section, as we focus here on the comparison of LUMO levels of the dopants. Similar to F4TCNQ, E_{red1} and E_{red2} for the ester analogues can be assigned to the formation of anion radicals from the neutral molecules and the formation of dianions from the anion radicals, respectively. Therefore, we assign singly and doubly reduced dopants as compound$^{\bullet-}$ and compound^{2-}, respectively. Among the compounds considered, F4TCNQ shows the deepest LUMO level, F4MCTCNQ$^{\bullet-}$ and F4OCTCNQ$^{\bullet-}$ show the next deepest levels, and F4DMCDCNQ$^{\bullet-}$ and F4DOCDCNQ$^{\bullet-}$ show relatively shallow levels. In addition, doubly reduced dopants show weaker reduction strength (smaller EA) and thereby shallower LUMO levels than singly reduced dopants, as expected. Another highlight of the CV measurements is that there is only one reduction peak for diester-substituted dopants. Thus, the LUMO levels of F4DMCDCNQ^{2-} and F4DOCDCNQ^{2-} are not shown because these species do not form based on the CV data. This suggests that the diester-substituted dopants undergo a different chemical process during reduction than the F4TCNQ and monoester-substituted dopants, the details of which will be discussed below. Finally, only subtle differences in LUMO levels are found between the methyl ester and octyl ester analogues, merely 0.01−0.04 eV, indicating that the R group on the ester does not strongly influence the electronic nature of the TCNQ dopants.

A mechanism is proposed to explain the charge transfer processes of F4TCNQ and ester-substituted dopants, as illustrated schematically in Figure 4. Assuming only one electron is involved at each step, radical anions are formed from neutral molecules in the first reduction. Resonance structures are also shown. Due to the molecular symmetry of the F4TCNQ and the diester molecules, the two resonance structures of their anion radicals are identical, whereas for the monoester molecules, the spin and negative charge density may be asymmetrically distributed. By accepting a second electron, dianions are formed subsequently for F4TCNQ and the monoesters. However, this is not the case for the diester molecules. Instead, radical coupling takes place to give a dimeric dianion. Only one reduction potential is observed, suggesting that the radical coupling is rapid and irreversible.

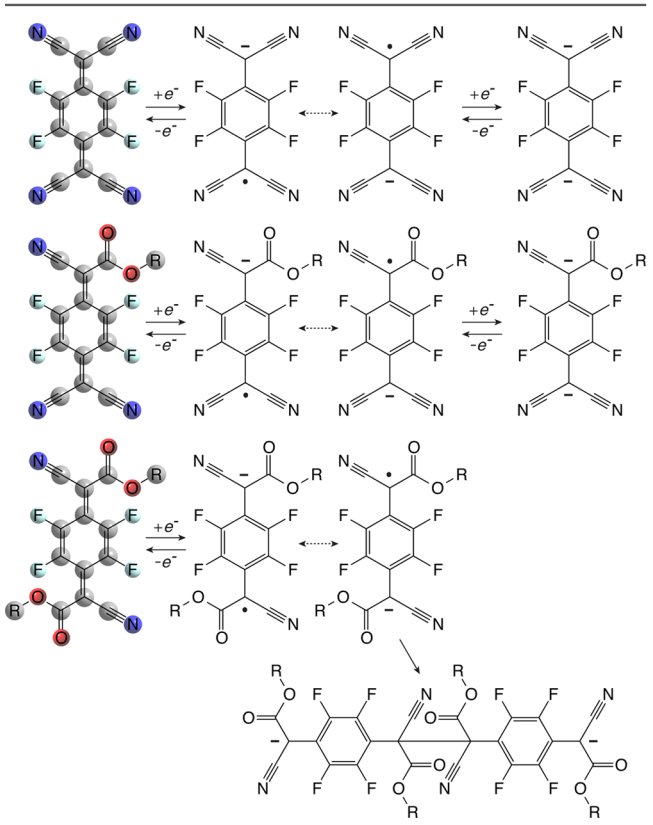

Figure 4. Proposed mechanism for charge transfer for F4TCNQ and its derivatives. The −R group can be a methyl or octyl group. Resonance structures for the radical anions are also displayed.

To support the above hypothesis, we measured the masses of the fully reduced dopant molecules using mass spectrometry (MS). F4TCNQ and all four ester-substituted analogues were mixed with potassium iodide (KI) to ensure full reduction, and the resulting mass spectra are shown in the Figures S37−S46. From these data, it is clear that diester dopants form dimers after reductionk while monoester dopants and F4TCNQ do not. The structure of the dimer shown in Figure 4 is a proposal based on the most likely site for spin coupling, involving no interference with the aromaticity of the benzene rings and with maximum possible separation of the charges. However, for the purposes of this work, the exact structure of the dimer is of no real consequence.

Characterization of Doped Films. It has been shown in the above sections that F4TCNQ can be synthetically altered to incorporate esters in place of nitrile groups, where the ester can support different alkyl chains that can be used to affect the solubility of the molecule. In this section we demonstrate successful p-type doping of the well-characterized conjugated polymer P3HT by the above-described ester-substituted dopants. In particular, we investigate the effect of altering the solubility of the dopant on the charge density and conductivity of the polymer.

Measuring Charge Density. Absorption spectroscopy (UV−vis−NIR) is commonly used to observe changes in the crystalline to amorphous content of P3HT samples.[50,51] The doping level can also be monitored using UV−vis−NIR.[30] Grazing incidence X-ray spectra and concentration-dependent conductivity were recently measured for the P3HT/F4TCNQ system.[52] For doping levels below 4 mol %, F4TCNQ occupies locations within the amorphous part of the P3HT[52] but dopes exclusively in the crystalline domains.[20] Between 4 mol % and 17 mol % doping ratios, F4TCNQ intercalates between the P3HT chains within crystalline domains, increasing the (010) crystal spacing (along the π-stacking direction) from 3.83 to7.18 Å.[52] The 17 mol % blend ratio is the point when this blend system reaches the upper limit on both conductivity and low energy absorptivity (1−1.7 eV) according to literature.[52]

The normalized UV−vis−NIR absorption spectra for P3HT/dopant at selected doping ratios are shown in Figure 5. The full doping concentration series of UV−vis−-NIR spectra can be found in the Supporting Information (Figure S48). These data exactly reproduce the literature results for P3HT/F4TCNQ.[52] Undoped P3HT has a band gap of ∼1.9 eV. Upon oxidation by F4TCNQ, two broad sub-bandgap absorbance peaks centered around 0.4 and 1.5 eV are observed, which can be assigned to the polarons of P3HT.[53,54] In addition, two sharper peaks at 1.43 and 1.62 eV can be detected that correspond to absorbance by F4TCNQ$^{\bullet-}$. As shown in Figure 5, subgap absorptions similar to those of F4TCNQ$^{\bullet-}$ are seen in F4MCTCNQ$^{\bullet-}$ and F4OCTCNQ$^{\bullet-}$. The double peaks at 1.43 and 1.62 eV are replaced by a single absorbance at the

DOI: 10.1021/acs.chemmater.5b02340
Chem. Mater. XXXX, XXX, XXX−XXX

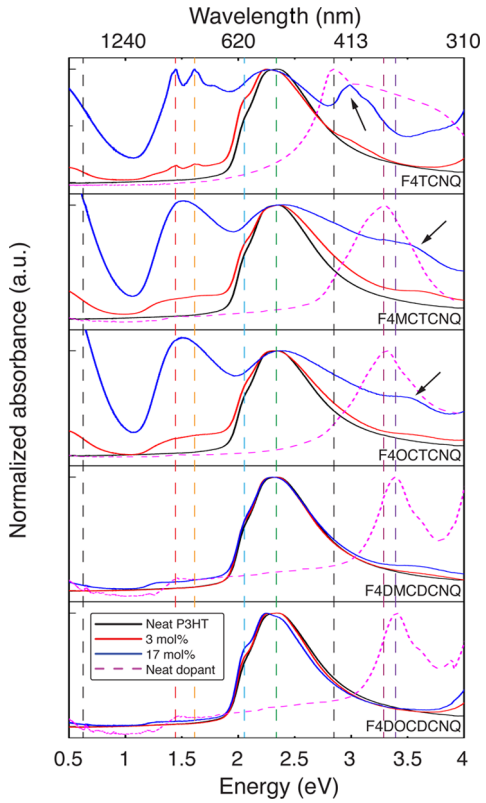

Figure 5. Normalized UV−vis−NIR absorbance spectra of neat P3HT (black), dopants (magenta dashed line), and P3HT/dopant blend films at 3 mol % (red) and 17 mol % (blue) doping ratios. Arrows show the dedope peak for P3HT/dopant system.

same energy that increases with increased dopant concentration. In fact, the NIR absorbance is stronger at both 0.4 and 1.5 eV in films doped with the monoester dopants than with F4TCNQ at the same mol % doping concentration. For instance, at 17 mol % the ratios between polaron absorbance at 1.5 eV to ground-state absorbance at 2.3 eV are 1:1, 1.04:1, and 1.12:1 for F4TCNQ, F4MCTCNQ and F4OCTCNQ, respectively. The increased polaron/ground-state ratio is an indication that higher P3HT polaron density is achieved for monoester derivatives. Conversely, only a slight increase in P3HT polaron peaks is observed in films containing F4DMCDCNQ and F4DOCDCNQ, even as the doping concentration reaches 17 mol %. This result indicates that there is less charge transfer between P3HT and the diester dopants compared with the F4TCNQ and monoester dopants at the same doping concentration.

Changes in the short-range ordered regions (aggregates)[55,56] of P3HT can be probed by monitoring the absorbance ratio of the 0−0 to 0−1 vibronic peaks at 2.03 eV (610 nm) and 2.25 eV (550 nm) because these peak are associated with interchain-delocalized excitation[47,57] and the degree of P3HT ordering.[55,58,59] The concentration-dependent spectra in the Figure S48 show that the relative intensity of the peak at 610 nm compared to the other P3HT vibronic peaks increases with increasing doping concentration up to 10 mol %. This result implies one of two things. It could indicate that crystalline domains of P3HT are becoming more ordered (more planar) upon doping. Alternatively, the relative increase in the peak at 2.03 eV could indicate an increased probability of doping in less crystalline domains. The ground-state signal is bleached upon doping and only the most crystalline sections of the sample are isolated from contact with the dopants. A relative increase in the peak at 610 nm occurs in all P3HT/acceptor systems, although the diester dopants induce less pronounced shifts in the vibronic spectra.

Besides the characteristics of the doping effects mentioned above, UV−vis−NIR spectra for all neat dopants are also presented. The absorbance spectra of these five dopants do not show many differences other than the broader and red-shifted absorption peak for F4TCNQ. The blueshift of the absorption peak from F4TCNQ (~2.8 eV) to the monoester derivatives (~3.3 eV) and diester derivatives (~3.4 eV) is expected due to less delocalization of charge resulting from replacing cyano with ester groups. The appearance of an additional peak in the high energy range of blend systems is also noted, as indicated by arrows (Figure 5). These peaks are assigned to the dopant anion, although in monoester systems an overlapping of the monoester anion absorbance and neutral dopant molecule absorbance is observed. A recent study from our group showed that this optical transition can be used to dedope P3HT/F4TCNQ films with complete recovery of optical characteristics and mobilities.[60] The related transitions for ester-substituted dopants are blue-shifted with respect to F4TCNQ by ~0.5 eV. The UV−vis−NIR spectra of the dopant anions can be found in the Figure S49.

The differential solubility of the mono- and diester dopants with methyl and octyl chains enables us to evaluate the effect of dopant solubility on doping efficiency, with the long chain esters showing higher solubility. Comparison of the $P3HT^{+}$/$dopant^{-}$ CT-state absorbance features to the ground-state absorbance of bulk P3HT gives a direct measure of the charge density. The results in this section clearly indicate that a dopant that is more miscible in the polymer has a higher probability of doping the polymer.

Measuring Dopant Miscibility. Photoluminescence spectroscopy (PL) is another technique that has been extensively used to evaluate doping interactions in organic materials because photoluminescence is quenched by the presence of dopants.[53,61] Dopants increase the free charge density in the polymer and free charges react with and quench excitons through a dark process with $\sim 1/r^3$ distance dependence.[62] PL experiments were performed using 2.4 eV excitation to optically excite P3HT and the PL emission for undoped P3HT (1.4−2.0 eV) was observed. Figure 6 shows the PL intensity as a function of mol fraction for all dopants. The inset shows typical PL spectra for neat and doped P3HT at 1 mol % doping ratio. As can be seen, F4DMCDCNQ and F4DOCDCNQ show only partial PL quenching of ~20% and ~40%, respectively. F4TCNQ is a stronger exciton quencher (~80%), whereas monoester dopants F4MCTCNQ and F4OCTCNQ are able to fully quench PL. This result clearly indicates that 20% of the P3HT volume remains undoped by F4TCNQ at 1 mol % doping ratio, while all P3HT domains are infiltrated by monoester-substituted dopants at the same concentration. The full concentration series of PL spectra can be found in the Figure S48. Unlike the monoester dopants where complete quenching occurs at lower than 1 mol % doping, complete quenching for diester dopants is observed at around 17 mol %. This is consistent with dimerization of the dopants, which causes charging of P3HT at higher dopant concentrations.

To summarize, on the basis of the reduction potential of the dopants, F4TCNQ should be a more effective dopant than the mono- and diester dopants by 0.2 and 0.4 eV, respectively.

DOI: 10.1021/acs.chemmater.5b02340
Chem. Mater. XXXX, XXX, XXX−XXX

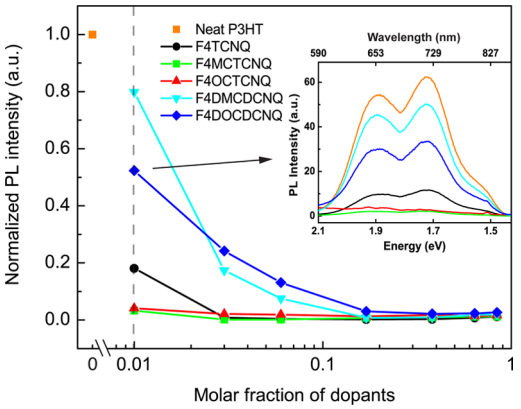

Figure 6. Normalized photoluminescence intensity as a function of doping concentration for all P3HT/dopant systems. Inset: PL quenching at 1 mol % doping ratio. The full doping concentration series of spectra can be found in the Supporting Information.

However, UV−vis−NIR results indicate that monoester-substituted TCNQs generate more charge density in P3HT at the same doping ratio. PL quenching demonstrates that monoester dopants infiltrate all domains of P3HT at a lower concentration than F4TCNQ. These results are in consistent with the increased solubility of dopants in $CHCl_3$.

Conductivity. In this section, we describe concentration-dependent conductivity measurements that were performed to determine whether the increase in dopant miscibility translates to enhanced electronic properties. Figure 7a shows a log−log plot of conductivity versus mole fraction of dopant for P3HT doped with F4TCNQ and each of the new dopants. Blend films at different doping ratios were spin-cast on prepatterned substrates and then measured by the four-point probe method, the details of which have been described in earlier publications.[63,64] It is clear that the in-plane conductivity of P3HT can be tuned by at least 3 orders of magnitude by all dopants. All dopants also show a similar trend of increased conductivity with increasing dopant concentration. After reaching a peak, the addition of more dopant leads to an increase in neutral dopant domains and conductivity decreases with increased concentration. The upper limit of conductivity in P3HT when doped with F4TCNQ or monoester dopants is ~10° S/cm while for diester dopants the maximum conductivity is ~1 × 10^{-1} S/cm.

Over most of the doping range, the conductivity of P3HT doped with the monoester dopants is higher at the same mole fraction than P3HT doped with F4TCNQ, which is consistent with UV−vis−-NIR and PL measurement results. For comparison to the earlier work of Duong et al.,[52] the conductivity data are also plotted on a log linear scale (Figure 7b). Just as was seen for P3HT doped with F4TCNQ, there is a clear change in the slope of conductivity vs concentration for all dopants at around 4 mol % dopant loading. We assume here that the assignments made by Duong et al. are correct in that the initial high slope comes from dopants mixing into the amorphous P3HT domains.[20,52] At higher doping ratios, the dopants intercalate into the crystalline P3HT domains, increasing the crystal spacing between P3HT chains. The initial slopes for loading of dopant up to 4 mol % are identical for the monoester dopants and F4TCNQ. However, when the doping ratio is increased beyond 4 mol %, F4OCTCNQ in particular shows a larger increase in conductivity with increased

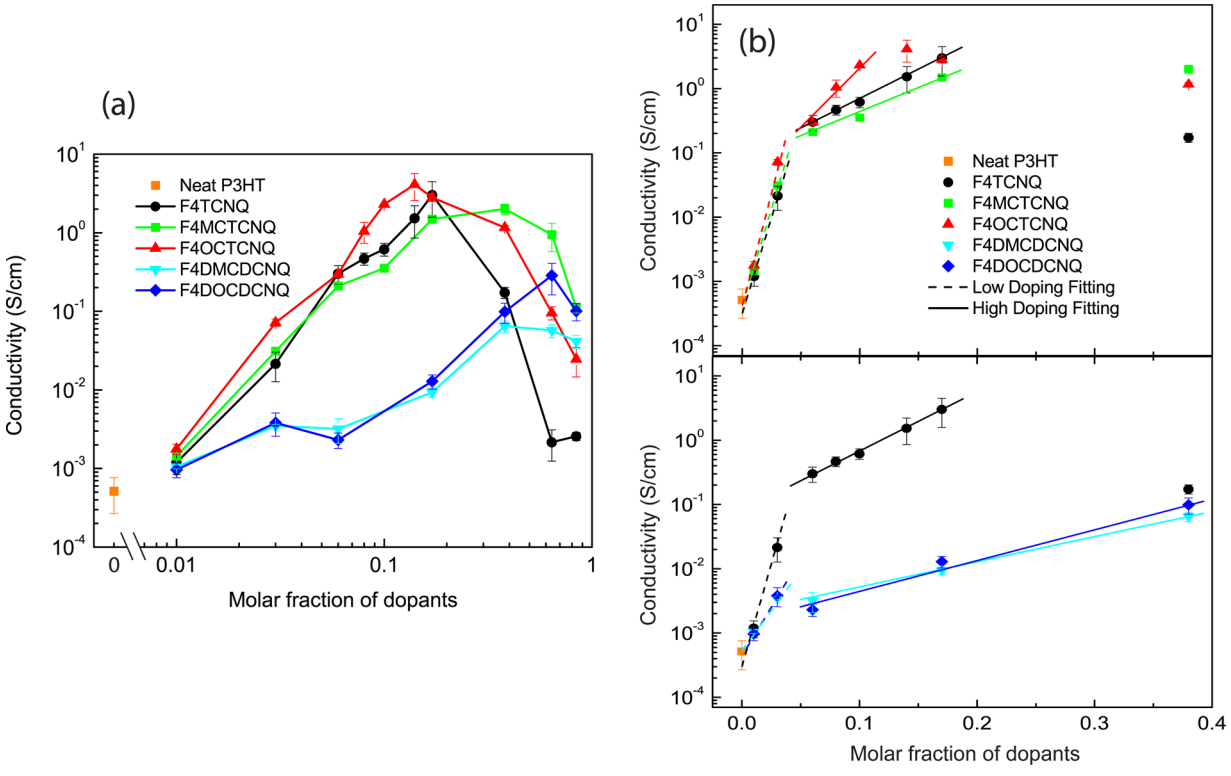

Figure 7. (a) In-plane conductivity measurements of P3HT/dopant blend films as a function of doping concentration. The neat P3HT film conductivity is also shown (orange). (b) Fits to the conductivity data in the weak (dashed lines) and strong (solid lines) doping regimes for F4TCNQ and the monoester derivatives (top) and diester derivatives (bottom).

DOI: 10.1021/acs.chemmater.5b02340
Chem. Mater. XXXX, XXX, XXX−XXX

doping than F4TCNQ, confirming that the modified dopant is more efficient at intercalating between P3HT chains. This result demonstrates that increased miscibility of the dopant has a clear advantage for doping efficiency. For F4TCNQ, the peak in conductivity occurs at 17 mol % doping followed by a rapid drop in conductivity with increased dopant concentration, presumably because increased dopant content is neutral and pure F4TCNQ crystals are formed in the polymer.[52] By comparison, both monoester dopants show a much broader peak in conductivity with increased dopant concentration, which also argues for better miscibility between the dopant and P3HT.

Another interesting observation is that the conductivity of P3HT samples doped with diester dopants increases exponentially up to 40 mol % doping ratio, whereas the F4TCNQ and monoester dopants show an exponential increase in conductivity until 10 mol % for F4OCTCNQ and 17 mol % for F4MCTCNQ and F4TCNQ, respectively. This is consistent with the UV−vis−NIR results for the diesters (Figure S48) which show that P3HT polaron density continues to increase with up to 64 mol % dopant loading. This trend cannot be explained solely by the relatively shallow LUMO level of diesters. Instead, the increase in conductivity with such high doping levels implies that the dimerization reaction stabilizes the doped states. The conductivity does not increase until there is high enough dopant concentration that they are able to dimerize and form stable dianions. This dimerization reaction shifts equilibrium toward the dianion, which is trapped by the irreversibility of the process and then cannot give the electron back into the polymer. Although it may be considered disadvantageous that large doping ratios are necessary to achieve higher conductivity with the diesters, there is a possible processing advantage to the dimerization reaction. This advantage is that the large dianion is unlikely to diffuse with thermal stress or drift with electric field stress. The smaller F4TCNQ is known to diffuse against a concentration gradient and thereby to dope regions of the sample outside of the originally intended area, thus reducing device lifetimes.[35] In addition, because the diester-substituted dopants do not dimerize until after deposition, they can be efficiently mixed into the polymer and then doping can occur post film formation through the dimerization reaction. The dopants, once dimerized, will provide a much higher barrier to diffusion.

CONCLUSIONS

In conclusion, we have developed a method to introduce solubility control into p-type organic dopants based on the F4TCNQ structure. Solubility control is achieved by replacing cyano groups on the F4TCNQ framework with ester groups. The results show that the solubility of the new ester dopants is improved by a factor of at least 30 and up to 100 compared with F4TCNQ at room temperature. In addition, these new dopants possess a range of interesting properties. First, monosubstituted ester dopants show only slightly lower (∼0.2 eV) electron affinity than F4TCNQ. However, in spite of the lower EA, monoester dopants lead to increased polaron density and more efficient doping in P3HT than F4TCNQ. F4OCTCNQ, for instance, has the same conductivity at 10 mol % doping as F4TCNQ at 17 mol % doping. The increased doping efficiency is proposed to be a result of the ester-substituted dopants being both more soluble in good solvents for P3HT and more miscible in P3HT itself. This study not only shows that molecular tailoring of organic dopants for increased miscibility with the desired polymer is a sound approach to improving doping efficiency, but also that single ester replacements are a viable method to modify common dopant structures with cyano attachments. Additionally, we also introduce diester-substituted dopants, which have distinctly different electrochemical properties than F4TCNQ and the monoester dopants due to a dimerization reaction that occurs between their radical anions. Despite the shallow LUMO level of the diesters, this irreversible dimerization also results in effective doping. However, much higher doping levels are needed for these diester dopants to maximize conductivity in P3HT, as shown by increased polaron density in optical spectra. Viewed broadly, these results provide a pathway for future dopant molecule design with controlled solubility/miscibility as a synthetic design parameter. Future studies will include a variety of ester −R groups that could tailor the placement of molecular dopants with respect to particular conjugated molecules/polymers.

ASSOCIATED CONTENT

Supporting Information

The Supporting Information is available free of charge on the ACS Publications website at DOI: 10.1021/acs.chemmater.5b02340.

Detailed synthetic procedures and NMR, mass, UV−vis, and photoluminescence spectra (PDF)

AUTHOR INFORMATION

Corresponding Authors

*E-mail: mjmascal@ucdavis.edu.

*E-mail: amoule@ucdavis.edu.

Author Contributions

†J.L. and G.Z. contributed equally to this work

Notes

The authors declare no competing financial interest.

ACKNOWLEDGMENTS

This research project was supported by the U.S. Department of Energy, Office of Basic Energy Sciences, Division of Materials Sciences and Engineering, under Award DE-SC0010419.

REFERENCES

(1) Forrest, S. R. The path to ubiquitous and low-cost organic electronic appliances on plastic. *Nature* **2004**, *428*, 911−918.

(2) Gunes, S.; Neugebauer, H.; Sariciftci, N. S. Conjugated Polymer-Based Organic Solar Cells. *Chem. Rev.* **2007**, *107*, 1324−1338.

(3) Cheng, Y.-J.; Yang, S.-H.; Hsu, C.-S. Synthesis of Conjugated Polymers for Organic Solar Cell Applications. *Chem. Rev.* **2009**, *109*, 5868−5923.

(4) Lussem, B.; Riede, M.; Leo, K. Doping of organic semiconductors. *Phys. Status Solidi A* **2013**, *210*, 9−43.

(5) Zhou, X.; Blochwitz, J.; Pfeiffer, M.; Nollau, A.; Fritz, T.; Leo, K. Enhanced Hole Injection into Amorphous Hole-Transport Layers of Organic Light-Emitting Diodes Using Controlled p-Type Doping. *Adv. Funct. Mater.* **2001**, *11*, 310−314.

(6) Reineke, S.; Thomschke, M.; Lüssem, B.; Leo, K. White organic light-emitting diodes: Status and perspective. *Rev. Mod. Phys.* **2013**, *85*, 1245−1293.

(7) Taima, T.; Sakai, J.; Yamanari, T.; Saito, K. Doping effects for organic photovoltaic cells based on small-molecular-weight semiconductors. *Sol. Energy Mater. Sol. Cells* **2009**, *93*, 742−745.

DOI: 10.1021/acs.chemmater.5b02340
Chem. Mater. XXXX, XXX, XXX−XXX

(8) Hains, A. W.; Liang, Z.; Woodhouse, M. A.; Gregg, B. A. Molecular Semiconductors in Organic Photovoltaic Cells. *Chem. Rev.* **2010**, *110*, 6689−6735.
(9) Braga, D.; Horowitz, G. High-Performance Organic Field-Effect Transistors. *Adv. Mater.* **2009**, *21*, 1473−1486.
(10) Lu, G.; Blakesley, J.; Himmelberger, S.; Pingel, P.; Frisch, J.; Lieberwirth, I.; Salzmann, I.; Oehzelt, M.; di Pietro, R.; Salleo, A.; Koch, N.; Neher, D. Moderate doping leads to high performance of semiconductor/insulator polymer blend transistors. *Nat. Commun.* **2013**, *4*, 1588.
(11) Heeger, A. J.; Sariciftci, N. S.; Namdas, E. B. *Semiconducting and Metallic Polymers*; Oxford University Press: Oxford, U.K., 2010.
(12) Jonsson, S.; Birgerson, J.; Crispin, X.; Greczynski, G.; Osikowicz, W.; van der Gon, A. D.; Salaneck, W.; Fahlman, M. The effects of solvents on the morphology and sheet resistance in poly(3,4-ethylenedioxythiophene)-polystyrenesulfonic acid (PEDOT-PSS) films. *Synth. Met.* **2003**, *139*, 1−10.
(13) Elschner, A.; Kirchmeyer, S. *PEDOT-Type Materials in Organic Solar Cells*; Wiley−vch: Weinheim, Germany, 2008.
(14) Walzer, K.; Maennig, B.; Pfeiffer, M.; Leo, K. Highly Efficient Organic Devices Based on Electrically Doped Transport Layers. *Chem. Rev.* **2007**, *107*, 1233−1271.
(15) Brédas, J.; Wudl, F.; Heeger, A. Polarons and bipolarons in doped polythiophene: A theoretical investigation. *Solid State Commun.* **1987**, *63*, 577−580.
(16) Colaneri, N.; Nowak, M.; Spiegel, D.; Hotta, S.; Heeger, A. J. Bipolarons in poly(3-methylthiophene): Spectroscopic, magnetic, and electrochemical measurements. *Phys. Rev. B: Condens. Matter Mater. Phys.* **1987**, *36*, 7964−7968.
(17) Aziz, E.; Vollmer, A.; Eisebitt, S.; Eberhardt, W.; Pingel, P.; Neher, D.; Koch, N. Localized Charge Transfer in a Molecularly Doped Conducting Polymer. *Adv. Mater.* **2007**, *19*, 3257−3260.
(18) Panda, P.; Veldman, D.; Sweelssen, J.; Bastiaansen, J. J. A. M.; Langeveld-Voss, B. M. W.; Meskers, S. C. J. Charge Transfer Absorption for -Conjugated Polymers and Oligomers Mixed with Electron Acceptors. *J. Phys. Chem. B* **2007**, *111*, 5076−5081.
(19) Zhu, L.; Kim, E.-G.; Yi, Y.; Brédas, J.-L. Charge Transfer in Molecular Complexes with 2,3,5,6-Tetrafluoro-7,7,8,8-tetracyanoquinodimethane (F4-TCNQ): A Density Functional Theory Study. *Chem. Mater.* **2011**, *23*, 5149−5159.
(20) Gao, J.; Roehling, J. D.; Li, Y.; Guo, H.; Moule, A. J.; Grey, J. K. The effect of 2,3,5,6-tetrafluoro-7,7,8,8-tetracyanoquinodimethane charge transfer dopants on the conformation and aggregation of poly(3-hexylthiophene). *J. Mater. Chem. C* **2013**, *1*, 5638−5646.
(21) Kearns, D. R.; Tollin, G.; Calvin, M. Electrical properties of organic solids. II. Effects of added electron acceptor on metalfree phthalocyanine. *J. Chem. Phys.* **1960**, *32*, 1020−1025.
(22) Chen, E. C. M.; Wentworth, W. E. A comparison of experimental determinations of electron affinities of pi charge transfer complex acceptors. *J. Chem. Phys.* **1975**, *63*, 3183−3191.
(23) Cooper, C. D.; Frey, W. F.; Compton, R. N. Negative ion properties of fluoranil, chloranil, and bromanil: Electron affinities. *J. Chem. Phys.* **1978**, *69*, 2367−2374.
(24) Ferraris, J.; Cowan, D. O.; Walatka, V.; Perlstein, J. H. Electron transfer in a new highly conducting donor-acceptor complex. *J. Am. Chem. Soc.* **1973**, *95*, 948−949.
(25) Compton, R. N.; Cooper, C. D. Negative ion properties of tetracyanoquinodimethan: Electron affinity and compound states. *J. Chem. Phys.* **1977**, *66*, 4325−4329.
(26) Maitrot, M.; Guillaud, G.; Boudjema, B.; André, J. J.; Simon, J. Molecular materialbased junctions: Formation of a Schottky contact with metallophthalocyanine thin films doped by the cosublimation method. *J. Appl. Phys.* **1986**, *60*, 2396−2400.
(27) Krikor, H.; Nagels, P. Structural characterization and electrical conductivity of poly(phenylethynyl) copper doped with iodine and 2,3-dichloro-5,6-dicyano-p-benzoquinone. *Synth. Met.* **1989**, *29*, 109−114.
(28) Tolbert, L.; Edmond, C.; Kowalik, J. Charge-transfer doping of poly(3-alkyl-2,2′-bithiophene). *Synth. Met.* **1999**, *101*, 500−501.
(29) Pingel, P.; Schwarzl, R.; Neher, D. Effect of molecular p-doping on hole density and mobility in poly(3-hexylthiophene). *Appl. Phys. Lett.* **2012**, *100*, 143303.
(30) Wang, C.; Duong, D. T.; Vandewal, K.; Rivnay, J.; Salleo, A. Optical measurement of doping efficiency in poly(3-hexylthiophene) solutions and thin films. *Phys. Rev. B: Condens. Matter Mater. Phys.* **2015**, *91*, 085205.
(31) Koech, P. K.; Padmaperuma, A. B.; Wang, L.; Swensen, J. S.; Polikarpov, E.; Darsell, J. T.; Rainbolt, J. E.; Gaspar, D. J. Synthesis and Application of 1,3,4,5,7,8-Hexafluorotetracyanonaphthoquinodimethane (F6-TNAP): A Conductivity Dopant for Organic Light-Emitting Devices. *Chem. Mater.* **2010**, *22*, 3926−3932.
(32) Tietze, M. L.; Burtone, L.; Riede, M.; Lüssem, B.; Leo, K. Fermi level shift and doping efficiency in *p*-doped small molecule organic semiconductors: A photoelectron spectroscopy and theoretical study. *Phys. Rev. B: Condens. Matter Mater. Phys.* **2012**, *86*, 035320.
(33) Gao, Z. Q.; Mi, B. X.; Xu, G. Z.; Wan, Y. Q.; Gong, M. L.; Cheah, K. W.; Chen, C. H. An organic p-type dopant with high thermal stability for an organic semiconductor. *Chem. Commun.* **2008**, 117−119.
(34) Schulze, K.; Uhrich, C.; Schüppel, R.; Leo, K.; Pfeiffer, M.; Brier, E.; Reinold, E.; Bäuerle, P. Efficient Vacuum-Deposited Organic Solar Cells Based on a New Low-Bandgap Oligothiophene and Fullerene C60. *Adv. Mater.* **2006**, *18*, 2872−2875.
(35) Meerheim, R.; Olthof, S.; Hermenau, M.; Scholz, S.; Petrich, A.; Tessler, N.; Solomeshch, O.; Lüssem, B.; Riede, M.; Leo, K. Investigation of C60F36 as low-volatility p-dopant in organic optoelectronic devices. *J. Appl. Phys.* **2011**, *109*, 103102.
(36) Solomeshch, O.; Yu, Y. J.; Goryunkov, A. A.; Sidorov, L. N.; Tuktarov, R. F.; Choi, D. H.; Jin, J.-I.; Tessler, N. Ground-State Interaction and Electrical Doping of Fluorinated C60 in Conjugated Polymers. *Adv. Mater.* **2009**, *21*, 4456−4460.
(37) Falkenberg, C.; Olthof, S.; Rieger, R.; Baumgarten, M.; Muellen, K.; Leo, K.; Riede, M. The role of energy level matching in organic solar cells−Hexaazatriphenylene hexacarbonitrile as transparent electron transport material. *Sol. Energy Mater. Sol. Cells* **2011**, *95*, 927−932.
(38) Diouf, B. B.; Jeon, W. S.; Park, J. S.; Choi, J. W.; Son, Y. H.; Lim, D. C.; Doh, Y. J.; Kwon, J. H. High hole mobility through charge recombination interface in organic light-emitting diodes. *Synth. Met.* **2011**, *161*, 2087−2091.
(39) Lin, H.; Lin, W.; Chang, J.; Wu, C. Solution-processed hexaazatriphenylene hexacarbonitrile as a universal hole-injection layer for organic light-emitting diodes. *Org. Electron.* **2013**, *14*, 1204−1210.
(40) Veysel, A. V.; De Sio, A.; Riedel, D.; Deschler, F.; Como, E. D.; Parisi, J.; von Hauff, E. Molecular doping of low-bandgap-polymer:-fullerene solar cells: Effects on transport and solar cells. *Org. Electron.* **2012**, *13*, 290−296.
(41) Rainbolt, J. E.; Koech, P. K.; Polikarpov, E.; Swensen, J. S.; Cosimbescu, L.; von Ruden, A.; Wang, L.; Sapochak, L. S.; Padmaperuma, A. B.; Gaspar, D. J. Synthesis and characterization of p-type conductivity dopant 2-(3-(adamantan-1-yl)propyl)-3,5,6-trifluoro-7,7,8,8-tetracyanoquinodimethane. *J. Mater. Chem. C* **2013**, *1*, 1876−1884.
(42) Arias, A. C.; MacKenzie, J. D.; McCulloch, I.; Rivnay, J.; Salleo, A. Materials and Applications for Large Area Electronics: Solution-Based Approaches. *Chem. Rev.* **2010**, *110*, 3−24.
(43) Pinal, R. Effect of molecular symmetry on melting temperature and solubility. *Org. Biomol. Chem.* **2004**, *2*, 2692−2699.
(44) Andersson, M. R.; Berggren, M.; Inganaes, O.; Gustafsson, G.; Gustafsson-Carlberg, J. C.; Selse, D.; Hjertberg, T.; Wennerstroem, O. Electroluminescence from Substituted Poly(thiophenes): From Blue to Near-Infrared. *Macromolecules* **1995**, *28*, 7525−7529.
(45) D'Andrade, B. W.; Datta, S.; Forrest, S. R.; Djurovich, P.; Polikarpov, E.; Thompson, M. E. Relationship between the ionization and oxidation potentials of molecular organic semiconductors. *Org. Electron.* **2005**, *6*, 11−20.
(46) Gao, W.; Kahn, A. Controlled p-doping of zinc phthalocyanine by coevaporation with tetrafluorotetracyanoquinodimethane: A direct

DOI: 10.1021/acs.chemmater.5b02340
Chem. Mater. XXXX, XXX, XXX−XXX

and inverse photoemission study. *Appl. Phys. Lett.* **2001**, *79*, 4040−4042.
(47) Österbacka, R.; An, C. P.; Jiang, X. M.; Vardeny, Z. V. Two-Dimensional Electronic Excitations in Self-Assembled Conjugated Polymer Nanocrystals. *Science* **2000**, *287*, 839−842.
(48) Hwang, I.-W.; Moses, D.; Heeger, A. J. Photoinduced Carrier Generation in P3HT/PCBM Bulk Heterojunction Materials. *J. Phys. Chem. C* **2008**, *112*, 4350−4354.
(49) Lloyd, M. T.; Prasankumar, R. P.; Sinclair, M. B.; Mayer, A. C.; Olson, D. C.; Hsu, J. W. P. Impact of interfacial polymer morphology on photoexcitation dynamics and device performance in P3HT/ZnO heterojunctions. *J. Mater. Chem.* **2009**, *19*, 4609−4614.
(50) Bouman, M. M.; Havinga, E. E.; Janssen, R. A. J.; Meijer, E. W. Chiroptical Properties of Regioregular Chiral Polythiophenes. *Mol. Cryst. Liq. Cryst. Sci. Technol., Sect. A* **1994**, *256*, 439−448.
(51) Moulé, A. J.; Meerholz, K. Controlling Morphology in Polymer-Fullerene Mixtures. *Adv. Mater.* **2008**, *20*, 240−245.
(52) Duong, D. T.; Wang, C.; Antono, E.; Toney, M. F.; Salleo, A. The chemical and structural origin of efficient p-type doping in P3HT. *Org. Electron.* **2013**, *14*, 1330−1336.
(53) Yim, K. H.; Whiting, G. L.; Murphy, C. E.; Halls, J. J. M.; Burroughes, J. H.; Friend, R. H.; Kim, J.-S. Controlling Electrical Properties of Conjugated Polymers via a Solution-Based p-Type Doping. *Adv. Mater.* **2008**, *20*, 3319−3324.
(54) Pingel, P.; Neher, D. Comprehensive picture of p-type doping of P3HT with the molecular acceptor F4TCNQ. *Phys. Rev. B: Condens. Matter Mater. Phys.* **2013**, *87*, 115209.
(55) Noriega, R.; Rivnay, J.; Vandewal, K.; Koch, F. P. V.; Stingelin, N.; Smith, P.; Toney, M. F.; Salleo, A. A general relationship between disorder, aggregation and charge transport in conjugated polymers. *Nat. Mater.* **2013**, *12*, 1037−1043.
(56) Koch, F. P. V.; et al. The impact of molecular weight on microstructure and charge transport in semicrystalline polymer semiconductors-poly(3-hexylthiophene), a model study. *Prog. Polym. Sci.* **2013**, *38*, 1978−1989. Topical issue on Conductive Polymers.
(57) Clark, J.; Silva, C.; Friend, R. H.; Spano, F. C. Role of Intermolecular Coupling in the Photophysics of Disordered Organic Semiconductors: Aggregate Emission in Regioregular Polythiophene. *Phys. Rev. Lett.* **2007**, *98*, 206406.
(58) Chang, L.; Lademann, H. W. A.; Bonekamp, J.-B.; Meerholz, K.; Moulé, A. J. Effect of Trace Solvent on the Morphology of P3HT:PCBM Bulk Heterojunction Solar Cells. *Adv. Funct. Mater.* **2011**, *21*, 1779−1787.
(59) Roehling, J. D.; Arslan, I.; Moule, A. J. Controlling microstructure in poly(3-hexylthiophene) nanofibers. *J. Mater. Chem.* **2012**, *22*, 2498−2506.
(60) Jacobs, I. E.; Li, J.; Burg, S. L.; Bilsky, D. J.; Rotondo, B. T.; Augustine, M. P.; Stroeve, P.; Moulé, A. J. Reversible Optical Control of Conjugated Polymer Solubility with Sub-micrometer Resolution. *ACS Nano* **2015**, *9*, 1905−1912.
(61) Tsoi, W. C.; Spencer, S. J.; Yang, L.; Ballantyne, A. M.; Nicholson, P. G.; Turnbull, A.; Shard, A. G.; Murphy, C. E.; Bradley, D. D. C.; Nelson, J.; Kim, J.-S. Effect of Crystallization on the Electronic Energy Levels and Thin Film Morphology of P3HT:PCBM Blends. *Macromolecules* **2011**, *44*, 2944−2952.
(62) Ferguson, A. J.; Kopidakis, N.; Shaheen, S. E.; Rumbles, G. Quenching of Excitons by Holes in Poly(3-hexylthiophene) Films. *J. Phys. Chem. C* **2008**, *112*, 9865−9871.
(63) Mauger, S. A.; Li, J.; Ozmen, O. T.; Yang, A. Y.; Friedrich, S.; Rail, M. D.; Berben, L. A.; Moule, A. J. High work-function hole transport layers by self-assembly using a fluorinated additive. *J. Mater. Chem. C* **2014**, *2*, 115−123.
(64) Nardes, A. M.; Kemerink, M.; Janssen, R. A. J.; Bastiaansen, J. A. M.; Kiggen, N. M. M.; Langeveld, B. M. W.; van Breemen, A.; de Kok, M. M. Microscopic understanding of the anisotropic conductivity of PEDOT:PSS thin films. *Adv. Mater.* **2007**, *19*, 1196−1200.

DOI: 10.1021/acs.chemmater.5b02340
Chem. Mater. XXXX, XXX, XXX−XXX